ACS APPLIED ENERGY MATERIALS

www.acsaem.org Article

Natural Band Alignments and Band Offsets of Sb_2Se_3 Solar Cells

Huw Shiel, Oliver S. Hutter, Laurie J. Phillips, Jack E. N. Swallow, Leanne A. H. Jones, Thomas J. Featherstone, Matthew J. Smiles, Pardeep K. Thakur, Tien-Lin Lee, Vinod R. Dhanak, Jonathan D. Major, and Tim D. Veal*

Cite This: *ACS Appl. Energy Mater.* 2020, 3, 11617−11626 Read Online

ACCESS | Metrics & More | Article Recommendations | Supporting Information

ABSTRACT: Sb_2Se_3 is a promising material for use in photovoltaics, but the optimum device structure has not yet been identified. This study provides band alignment measurements between Sb_2Se_3, identical to that used in high-efficiency photovoltaic devices, and its two most commonly used window layers, namely, CdS and TiO_2. Band alignments are measured via two different approaches: Anderson's rule was used to predict an interface band alignment from measured natural band alignments, and the Kraut method was used in conjunction with hard X-ray photoemission spectroscopy to directly measure the band offsets at the interface. This allows examination of the effect of interface formation on the band alignments. The conduction band minimum (CBM) of TiO_2 is found by the Kraut method to lie 0.82 eV below that of Sb_2Se_3, whereas the CdS CBM is only 0.01 eV below that of Sb_2Se_3. Furthermore, a significant difference is observed between the natural alignment- and Kraut method-determined offsets for TiO_2/Sb_2Se_3, whereas there is little difference for CdS/Sb_2Se_3. Finally, these results are related to device performance, taking into consideration how these results may guide the future development of Sb_2Se_3 solar cells and providing a methodology that can be used to assess band alignments in device-relevant systems.

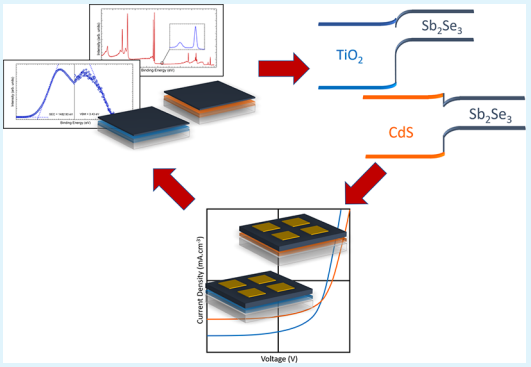

KEYWORDS: *Sb_2Se_3, band alignments, window layer, photovoltaics, photoemission, HAXPES*

INTRODUCTION

The field of solar energy has made great leaps forward in recent years, leading the charge for a switch from the unsustainable burning of fossil fuels to a green energy future. While technologies such as crystalline silicon and cadmium telluride (CdTe) thin films have achieved great success industrially, there is a need for additional technologies when striving to achieve terawatt scale. Antimony selenide (Sb_2Se_3) has all the desirable characteristics to be successful on an industrial level; it is a stable, binary compound made up of cheap and earth-abundant elements, has a direct band gap of 1.18 eV[1] and a very high absorption coefficient, $>10^5$ cm^{-1}.[2] Its unusual 1D nanoribbon structure allows for very effective carrier transport if the correct orientation is achieved and has also been suggested to allow the formation of benign grain boundaries.[3−5] Furthermore, the device performance has progressed rapidly since first being used in a solar cell,[6,7] reaching nearly 10% in 2019.[8,9]

These qualities make Sb_2Se_3 a very promising material. However, Sb_2Se_3 photovoltaics (PV) remains an emerging technology, with a significant amount of fundamental understanding still missing from the literature. The impact of this is felt particularly in the design of various device structures utilizing different window layers (Figure 1). Cadmium sulfide (CdS) and titanium dioxide (TiO_2) are both used frequently,

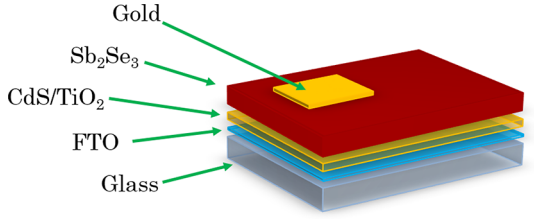

Figure 1. Schematic of the typical superstrate device structure used in Sb_2Se_3 solar cells.

with some studies finding CdS to offer superior performance[3,10,11] and others finding the switch to TiO_2 extremely beneficial.[4,12] There are many aspects of these alternative device structures that are not understood, particularly the role of band alignments in influencing the device performance.

Band alignment is a general term used to describe the way the valence and conduction bands of two materials line up to

Received: June 23, 2020
Accepted: December 2, 2020
Published: December 15, 2020

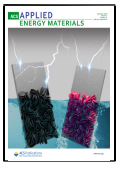

https://dx.doi.org/10.1021/acsaem.0c01477
ACS Appl. Energy Mater. 2020, 3, 11617−11626

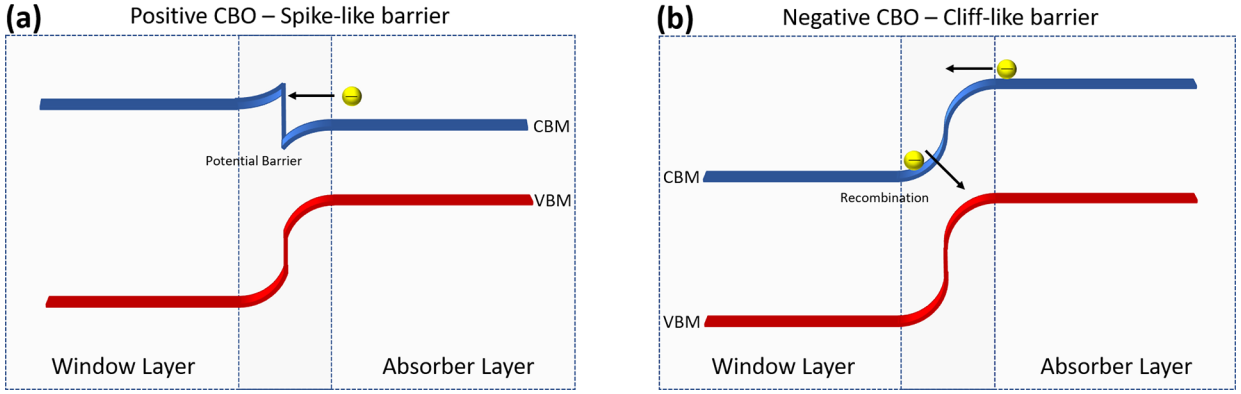

Figure 2. Schematic diagram showing (a) a very positive CBO leading to a potential barrier in the conduction band and (b) a very negative CBO leading to a recombination center and low built-in voltage.

perform a certain function. The "natural" band alignment of two materials describes the positions of the band extrema with respect to the vacuum level when not in contact with each other. The term band offset refers to the separation of the band extrema between the two materials once contacted. A "spikelike" band offset is defined as where the conduction band minimum (CBM) of the window layer lies above the CBM of the absorber and a "clifflike" offset as when the CBM of the window layer lies below that of the absorber. With too positive an offset (Figure 2a), electrons excited in the absorber will face a potential barrier opposing their drift into the window layer and lowering the short-circuit current (J_{sc}) (and efficiency) of the cell. Too negative a CBO (Figure 2b) leads to a potential source of back-transfer carrier recombination at the interface between the conduction band of the window layer and the valence band of the absorber. This recombination, in which electrons in the window layer recombine with holes in the absorber via interface states, is more likely the narrower the gap between the two energy levels.[13] A clifflike offset also limits the built-in voltage (V_{bi}) of the junction, leading to a lower open-circuit voltage (V_{oc}). The J_{sc} and V_{oc} are crucial aspects of the solar cell performance; therefore, it is vital that a good band alignment is obtained for a PV technology to be successful.[14,15]

One of the best ways to measure band alignments is through photoemission techniques such as X-ray photoemission spectroscopy (XPS). Through use of the valence band and secondary electron cutoffs in an XPS spectrum, the ionization potential and work function of a material can be measured relative to the vacuum level.[16,17] These quantities do not describe the interface itself, but via a method called Anderson's rule the band alignment can be predicted. Another technique often employed is the Kraut method,[18,19] which allows the direct measurement of valence band offset (VBO) between two materials. Both methods employ a number of assumptions that will be discussed below.

In this study, the powerful photoemission techniques of traditional laboratory-based XPS and synchrotron-based hard X-ray photoemission spectroscopy (HAXPES) were used to measure and compare band alignments using both Anderson's rule[20] and the Kraut method.[18] By examination of the differences between the two sets of results, conclusions can be drawn about the effect of interface formation on the two different band alignments. Furthermore, by comparing these results to previous device studies, we assess the influence and impact of the band alignments on device performance characteristics.

METHODS

Film Deposition. CdS films were deposited onto TEC10 fluorine-doped tin oxide (FTO)-coated glass substrates (supplied by NSG Group) by RF-magnetron sputtering at 60 W, 5 mTorr of Ar gas and a substrate temperature of 200 °C for 24 min. The CdS films were ∼80 nm thick as determined by an Ambios xp200 profilometer. Anatase TiO_2 films were deposited by a two-step process: first, an RF-magnetron sputtered film was deposited at room temperature at 150 W and 5 mTorr for 30 min, and second an established spin-casting process[21] was carried out for a total film thickness of ∼60 nm.

Sb_2Se_3 films were deposited by close-space sublimation (CSS) at a source temperature of 390 °C with substrate heating at 330 °C and a base pressure of ∼0.05 Torr. Interfacial films for band alignment measurements were deposited for only 30 s to achieve a film thin enough to carry out the Kraut method (∼20 nm). For the "bulk" samples, a thicker layer (∼50 nm) was deposited so that the signal from the layer beneath was not seen in the HAXPES measurements. Detailed structural characterization (including cross-sectional transmission electron microscopy and X-ray diffraction) of similar films can be found in the work by Williams et al.[5]

Photoemission. HAXPES measurements were carried out at the I09 beamline at Diamond Light Source, Oxfordshire, UK. A double-crystal Si(111) monochromator was used to select 5921 eV X-rays followed by a Si(004) channel-cut crystal, resulting in energy resolution of 0.25 eV (as determined by measuring the Fermi edge of a polycrystalline gold reference sample at room temperature and fitting a Gaussian-broadened Fermi−Dirac distribution to the data). This allowed binding energy determination with a precision better than ±0.1 eV. The spectra were acquired using a Scienta Omicron EW4000 high-energy analyzer with an acceptance angle of ±28°.

Laboratory-based XPS data were collected using a monochromated Al Kα X-ray source ($h\nu$ = 1486.6 eV) operating at 250 W and a PSP Vacuum Systems hemispherical electron energy analyzer with an acceptance angle of ±3° operating with a constant pass energy of 10 eV. The energy resolution was determined to be 0.4 eV from fitting a Gaussian-broadened Fermi−Dirac distribution to the Fermi edge of a polycrystalline silver reference sample,[22] allowing binding energy determination with a precision of ±0.1 eV.

All samples exhibited a small C 1s contaminant peak (and O 1s for the CdS sample) because of exposure to atmospheric conditions. The films were sufficiently conducting and were grounded to the spectrometer using a top electrical contact to avoid any surface-charging effects.

Measuring Band Alignments by Photoemission. The measurement of the natural band alignments via photoemission is a commonly used procedure when screening materials for use as a junction partner to an absorber in a PV device.[23,24] While most studies use ultraviolet photoemission spectroscopy (UPS), a highly surface-sensitive technique for studying work functions, it is also possible to use XPS, which is slightly less surface-sensitive (albeit still limited to the top few nanometers). This method involves measuring

https://dx.doi.org/10.1021/acsaem.0c01477
ACS Appl. Energy Mater. 2020, 3, 11617−11626

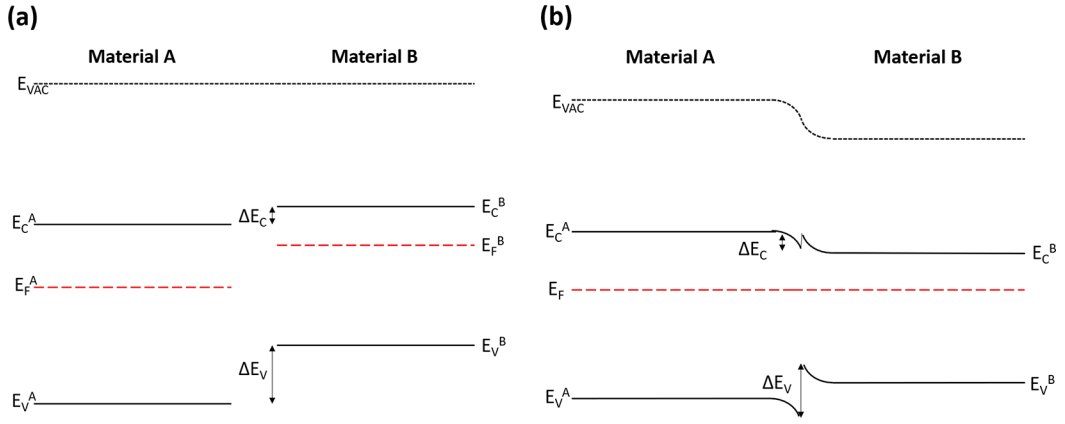

Figure 3. Schematic diagram of how band alignments are predicted using the Anderson rule with (a) showing the natural alignments referenced to the vacuum level and (b) showing band alignment after aligning Fermi levels.

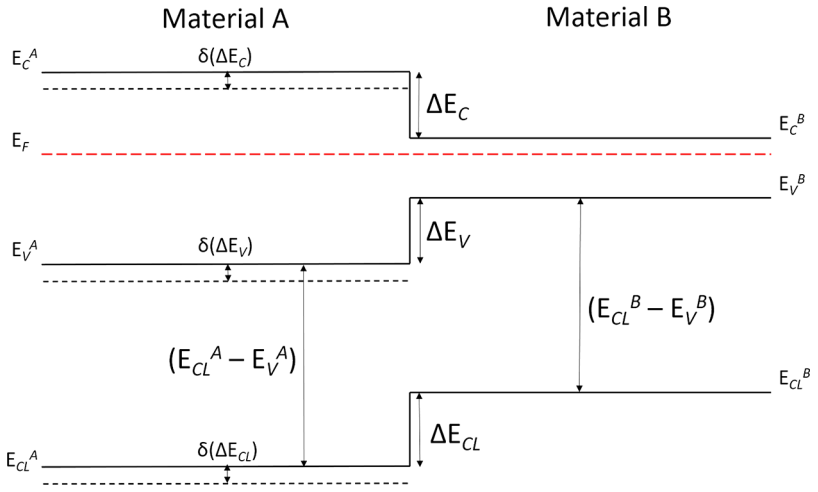

Figure 4. Schematic showing the band alignments measured by the Kraut method where δ signifies the band energy shift due to interface formation and ΔE signifies the band offsets.

the ionization potential of a material, which describes the position of the valence band maximum relative to the vacuum level, and then using either a measured or literature-quoted band gap to determine the electron affinity, which describes the position of the conduction band relative to the vacuum level. When measuring the ionization potential, taking advantage of the fact that all XPS spectra are referenced to the Fermi level, one can also determine the position of the Fermi level in the band gap. Knowing that when two semiconductors are contacted, the Fermi levels of the two must be aligned, there is a need for a model of how this affects the alignments of the conduction and valence bands at the interface.

Anderson's Rule. One widely used approach is known as Anderson's rule or the electron affinity rule.[20,23] This method states that the Fermi levels of the two materials align, while maintaining the difference in natural electron affinity at the interface (Figure 3). However, this method does not take into account the role of charge transfer, orientation, or interface-induced gap states upon contacting two materials. Therefore, if the two materials have significantly different electronegativities or lattice spacing, this approximation could differ significantly from the real band alignment.[23,25,26] It also relies either on some assumptions or complex additional measurements to determine how the band bending is distributed across the two sides of the interface.

The Kraut Method. The alternative method used in this study, the Kraut method,[18] uses a combination of measurements to take into account the charge transfer across the interface between two materials. First, the binding energy of high-intensity core (E_{CL}) levels and the VBM (E_V) are measured for both materials in vacuum. Then a film of one material is deposited onto the other, thin enough that photoelectrons from the lower layer can still escape and be detected during an XPS measurement. This allows an interface-sensitive measurement in which peaks from both materials are resolved. Then by measuring the separation between core levels in the two materials (ΔE_{CL}) and exploiting the fact that the core level shift upon interface formation is equal to the shift in the valence and conduction bands ($|\delta E_{CL}| = |\delta E_V| = |\delta E_C|$), the valence band offset between them can be directly determined, as shown in Figure 4 and eq 1:

$$\Delta E_V = (E_{CL}^B - E_V^B) - (E_{CL}^A - E_V^A) + \Delta E_{CL} \quad (1)$$

where A and B denote material A and material B and $\Delta E_{CL} = E_{CL}^A - E_{CL}^B$, in the interfacial sample. The key difference between the Kraut method and Anderson's rule, therefore, is that Anderson's rule is a prediction of the band alignment based on measurements of the separate materials, whereas the Kraut method is a direct measurement of the band offset, albeit with some simplifications. The Kraut method approach is an abrupt interface approximation, meaning that a single measurement gives only a single offset between the bands and, though the effects of band bending are accounted for, the band bending itself is not measured. Multiple measurements carried out during interface formation can provide more detailed measurements of the band bending; however, this requires simultaneous in situ deposition and photoemission measurements, something that is not possible while using deposition techniques such as close space sublimation (CSS). A drawback to this method, however, is sample preparation. As shown in Figure 5, the inelastic mean free path (IMFP) of a photoelectron is dependent on its kinetic energy, and according to the Beer–Lambert

https://dx.doi.org/10.1021/acsaem.0c01477
ACS Appl. Energy Mater. 2020, 3, 11617–11626

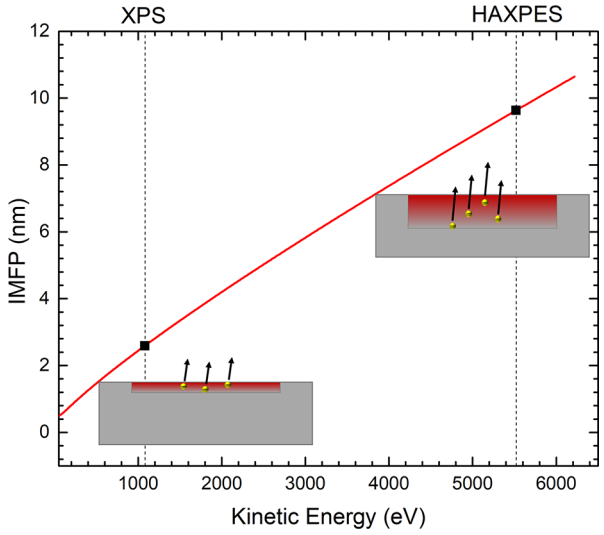

Figure 5. Inelastic mean free path of photoelectrons in Sb_2Se_3 with respect to kinetic energy.[29] Black points show the kinetic energy of an electron escaping the Sb 3d orbital for both conventional Al Kα XPS (1486.6 eV) and HAXPES (assuming a photon energy of 5921 eV) and the inset sketches illustrate the relative probing depths of the two techniques.

law, 95% of the signal originates within three IMFPs of the surface. Accordingly, the sampling depth of XPS is then roughly 10 nm, and a film thinner than this is required to carry out any Kraut method studies using conventional laboratory-based XPS.

Many of the recent advances in Sb_2Se_3 device performance have come via the use of CSS or vapor transport deposition (VTD) of Sb_2Se_3.[4,12,27,28] CSS allows for the formation of large grain sizes with good preferred orientation for carrier transport. This does, however, limit the thinness of films that can be deposited while still achieving good coverage, which is essential to the validity of the Kraut method measurements. At roughly 20 nm, good coverage is achievable by CSS and this falls well within the sampling depth (Figure 5) of HAXPES, a synchrotron-based technique that works by the same principle as conventional photoemission methods but with hard X-rays. With an excitation energy of 6000 eV, for example, the IMFP and effective probing depth of photoelectrons are greater than 9 and 27 nm respectively, for Sb_2Se_3 (as calculated using the TPP-2M equation[29]). With use of this method then, the band offset between a device-relevant layer of Sb_2Se_3 and a window layer can be directly measured. Combining this with natural alignments measurements can provide powerful insights into the formation of these interfaces simply by observing the differences between the two measurements.

Measurement of band alignments on material that was identical to that used in PV devices of good efficiency (>5%) was important to this study because the properties of Sb_2Se_3 are very sensitive to the deposition method and material quality.[4,12,30] The following section includes results from natural band alignment measurements, Kraut method band offset measurements, and a comparison to device performance characteristics. The films used for all three aspects of these results are directly comparable because they are all deposited from the same source material via the same deposition method. This is, to the best of our knowledge, the most device-relevant measurement of band alignments in Sb_2Se_3 solar cells performed to date. Through direct comparison of films and devices, this work provides a method by which improved window layer partners for Sb_2Se_3 solar cells can be identified.

RESULTS

Natural Alignments. Initially, we measured the ionization potential and work function of Sb_2Se_3, CdS, and TiO_2 films that were deposited under the same conditions used for fabrication of devices.[4,12] Figure 6 shows the secondary electron cutoff and valence band edge of TiO_2, CdS, and Sb_2Se_3 that are used to measure the valence band and Fermi level positions of each material with respect to the vacuum level. Each cutoff was fitted with a linear fit. As can be seen in Figure 6, while the gradients naturally vary between the samples, there are no unusual shapes to any of the cutoffs.

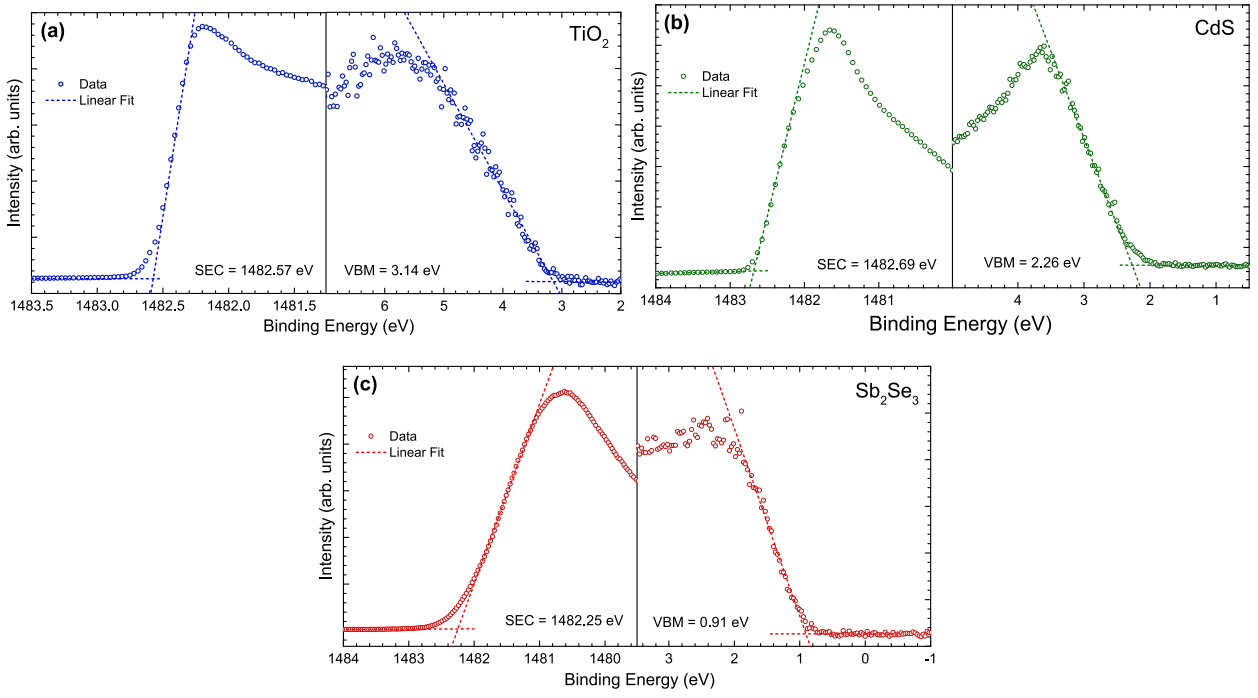

Figure 6. Secondary electron cutoff (SEC) and valence band maximum (VBM) obtained by XPS for "bulk" samples of (a) TiO_2, (b) CdS, and (c) Sb_2Se_3 with linear fits.

https://dx.doi.org/10.1021/acsaem.0c01477
ACS Appl. Energy Mater. 2020, 3, 11617−11626

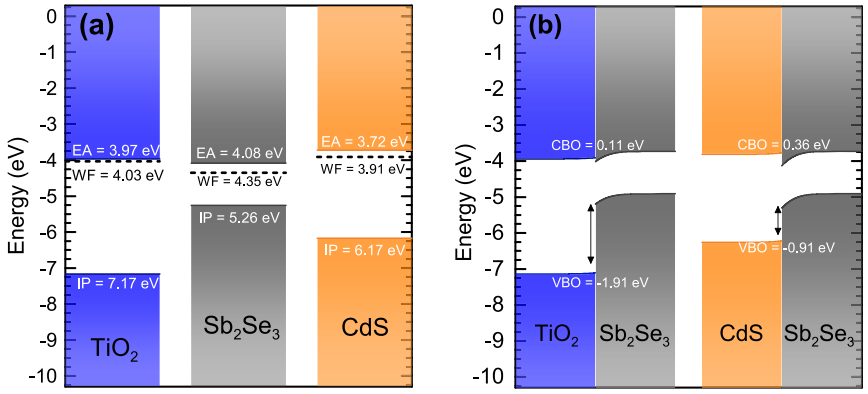

Figure 7. (a) Natural alignments of Sb_2Se_3 (gray) alongside TiO_2 (blue) and CdS (orange) with the Fermi levels aligned. (b) Band alignments when the Fermi levels of the window layers are aligned with that of Sb_2Se_3. The band gaps used for TiO_2, Sb_2Se_3, and CdS were 3.2, 1.18, and 2.45 eV, respectively.

With use of the data from Figure 6 and the literature band gap values,[1,31−33] the electron affinity of each material can be inferred and subsequently a band diagram drawn (Figure 7a). From Figure 7a it can be seen that all three materials are n-type. The n-type conductivity of Sb_2Se_3 is a result of the presence of chlorine impurities in the purchased source material—a more detailed discussion of n-type Sb_2Se_3 as well as the formation of an isotype heterojunction is provided by Hobson et al.[34]

Figure 7b shows the alignment between Sb_2Se_3 and TiO_2 and between Sb_2Se_3 and CdS if the Fermi levels are aligned according to Anderson's rule. According to this rule, the difference in electron affinity is fixed at the interface, leading to a small spike of 0.36 eV between CdS and Sb_2Se_3 and a smaller spike of 0.11 eV between TiO_2 and Sb_2Se_3. The bulk band positions of each material are determined from Figure 7a and are shifted up/down to align the Fermi levels. Band bending is then incorporated to resolve the discontinuity. An assumption has to be made regarding the distribution of the band bending—in this case it is almost entirely in the Sb_2Se_3 given that the majority of the band bending will occur in the material with the lowest carrier density[26] and that Sb_2Se_3 is known to undergo significant band bending at the surface.[34] From this it would appear that Sb_2Se_3 and CdS have a good alignment for effective carrier transport in a PV device—a small spike up to 0.4 eV is widely considered to be conducive to achieving high efficiencies[14,35,36] by maximizing available voltage and minimizing the chance of recombination while maintaining a CBO small enough for carriers to overcome.

Band Offset Measurements. The Kraut method approach takes into account the charge transfer between the two materials by directly measuring the interface between them. In this study, HAXPES was used to enhance the inelastic mean free path of the photoemitted electrons, thereby allowing us to measure band alignments with a thicker layer of Sb_2Se_3 (~20 nm). Figure 9 shows the photoemission data collected for the band alignment between Sb_2Se_3 and either CdS or TiO_2 (sample set shown in Figure 8). Figure 9a−c shows survey scans including insets of the detailed valence band scans used to determine VBM positions for each material. Figure 9d,e shows survey scans of the interfacial samples with insets showing the separately measured core levels from the window layers. Core level and VBM binding energies are included in Table S1 (Supporting Information). Detailed scans of the Ti, Cd, and Sb core levels used and the respective valence bands are included in the Supporting Information (Figures S1−S5).

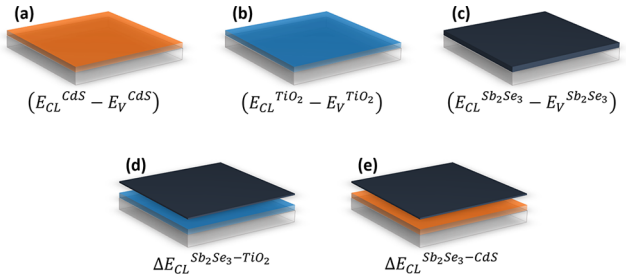

Figure 8. Sample set used for Kraut method band offset measurements along with quantities measured from each one: (a)−(c) show "bulk" samples of (a) CdS, (b) TiO_2, and (c) Sb_2Se_3 and (d) and (e) show "interfacial" samples of (d) Sb_2Se_3 on TiO_2 and (e) Sb_2Se_3 on CdS.

Figure 10a shows the band offsets drawn from the VBOs measured by the Kraut method using HAXPES of Sb_2Se_3 on both CdS and TiO_2. In the Kraut method approach, no bulk band positions are measured and the offsets acquired are representative of the interface only. The VBOs were obtained using a number of characteristic Sb_2Se_3 peaks (Sb 3d, Sb 4d, and Se 3d) but only one window layer peak was used as only the most intense one was resolvable (Cd 3d and Ti 2p) because of the attenuation of the window layer photoelectrons by the Sb_2Se_3 overlayer. The values presented in this work are an average of the VBOs calculated from the different core levels—the full breakdown of values is included in Table S2. The Sb_2Se_3/CdS interface has a small CBO of −0.01 eV. The band alignment between Sb_2Se_3 and TiO_2 corresponds to a large clifflike CBO of −0.82 eV. These appear significantly different than the natural alignment results at first glance. However, before the two measurements can be compared, the impact of the assumptions and approximations involved in the two approaches must be considered.

DISCUSSION

The measurement of the band offsets via the Kraut method assumes flat bands and an abrupt junction. However, we must consider which regions of the interface contribute most strongly to the photoemission spectra. From the weakness of the Ti 2p signal from the TiO_2 layer in Figure 9d (and similarly for Cd 3d from the CdS), it is clear that only a very thin part of

https://dx.doi.org/10.1021/acsaem.0c01477
ACS Appl. Energy Mater. 2020, 3, 11617−11626

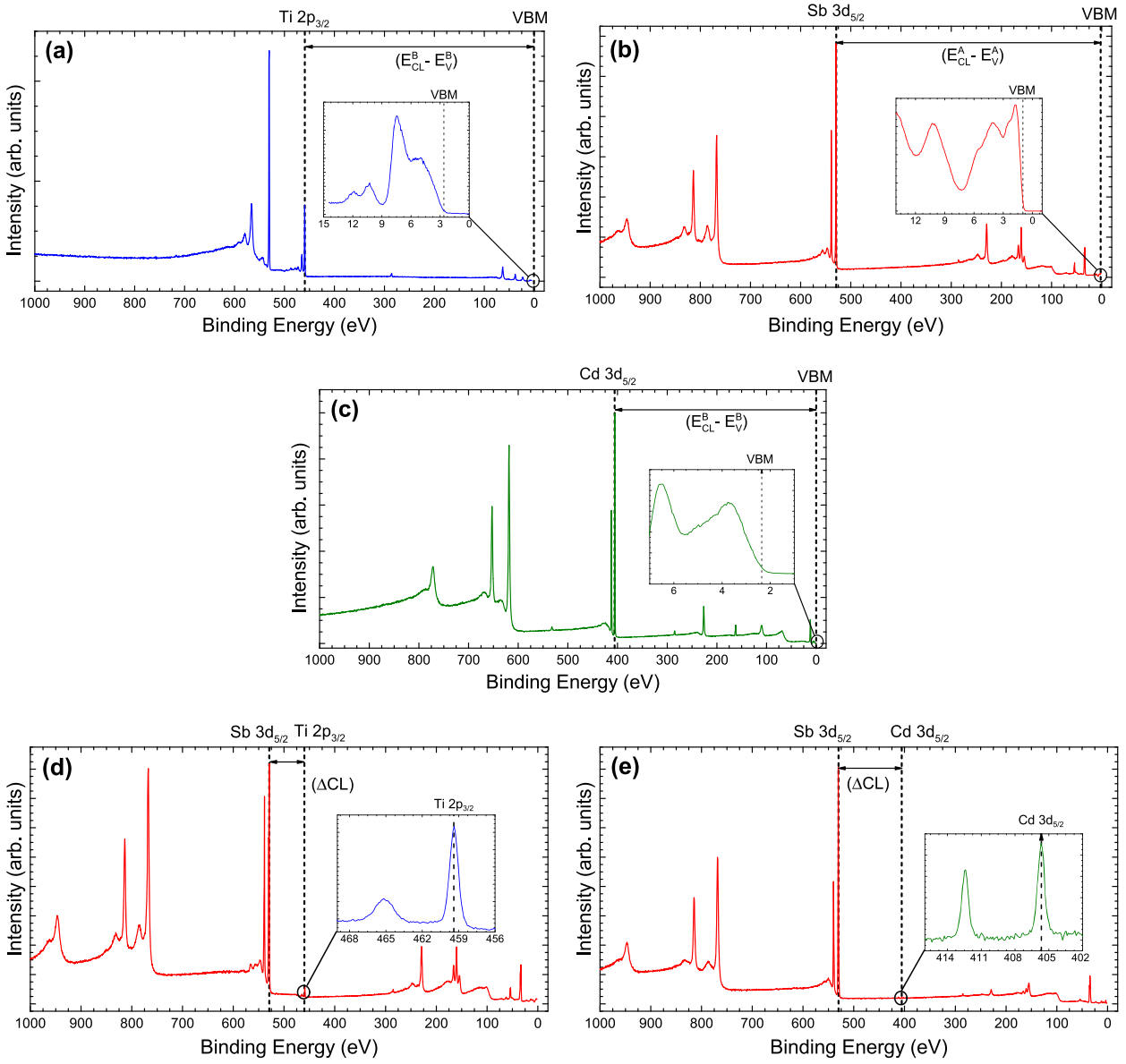

Figure 9. HAXPES data used to calculate band offsets. (a)−(c) show survey scans of "bulk" (a) TiO_2, (b) Sb_2Se_3, and (c) CdS with separately measured VBMs shown in insets. (d) and (e) show the "interfacial" samples of (d) Sb_2Se_3 on TiO_2 and (e) Sb_2Se_3 on CdS with the separately measured core level peaks from the substrates shown in the inset.

the window layer would be detected, right at the interface with Sb_2Se_3 (red circles in Figure 10b). For the Sb_2Se_3, we can be sure that the bulk band position (green circles in Figure 10b) will dominate the signal considering that, as shown in Figure 5, the Beer−Lambert law dictates that 63% of the signal will originate from the top 9 nm. This leads us to assume that the most relevant comparison between the natural alignments and the Kraut method is as depicted in Figure 10b. Figure 10b shows the same data as presented in Figure 7b, with colored circles to indicate the equivalent regions that would be probed by the Kraut method. The predicted offsets (CBO^P and VBO^P) presented in Figure 10b show the energy separation between these circled regions of the Sb_2Se_3 and respective window layers, for easy comparison with Figure 10a. Therefore, the predicted band offsets quoted in Figure 10b are not measured, but are rather a projection of what the interface predicted by Anderson's rule (Figure 7b), in the absence of interface charge transfer, would yield if measured via the Kraut method.

On the basis of this assumption, comparing parts (a) and (b) of Figure 10, we can see that for the CdS/Sb_2Se_3 interface there is very good agreement between the Kraut method and Anderson's rule. This strengthens the conclusion that CdS and Sb_2Se_3 have excellent band alignments for good device performance in photovoltaics and suggests that the band alignment between CdS and Sb_2Se_3 predicted by Anderson's rule is an accurate prediction of the true band alignment. However, for the TiO_2/Sb_2Se_3 interface, there is a significant difference between VBO and CBO given by the Kraut method and the modified Anderson's rule results. Even when taking into account the differences between the two approaches regarding band bending (Figure 10b), the predicted offset (CBO^P) between the flat band position in the Sb_2Se_3 and the edge of the TiO_2 band is only −0.18 eV in the modified Anderson model, compared to a CBO of −0.82 eV measured by the Kraut method. According to the Kraut method here, even with an equivalent amount of band bending as predicted

https://dx.doi.org/10.1021/acsaem.0c01477
ACS Appl. Energy Mater. 2020, 3, 11617−11626

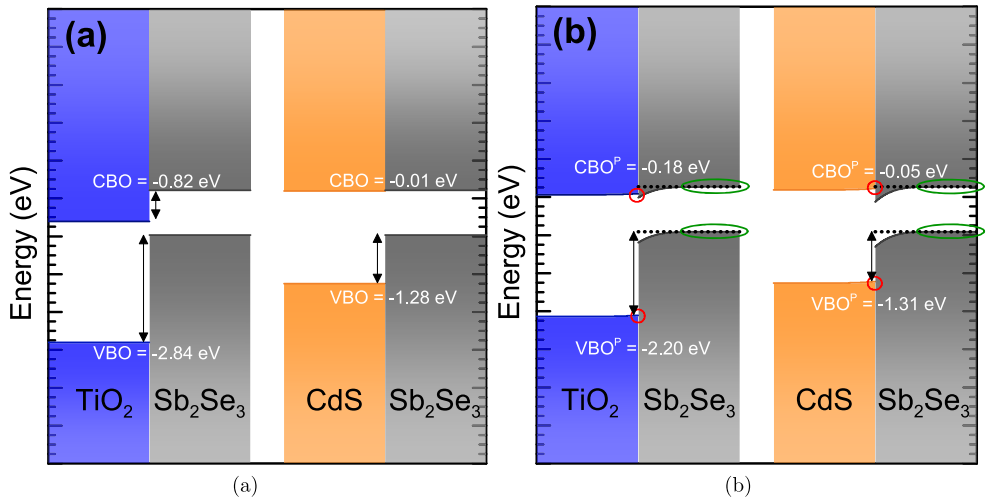

(a) (b)

Figure 10. (a) Band offsets measured via the Kraut method using HAXPES and (b) natural alignments calculated by Anderson's rule (Figure 7b), with red and green circles indicating the equivalent regions probed by the Kraut method in the window layer and Sb_2Se_3, respectively.

by Anderson's rule, the CBO would actually be clifflike at the interface (Figure 10a), rather than the 0.11 eV spike predicted by Anderson's rule (Figure 7b). This suggests that there is a large degree of charge transfer upon contact, which increases the VBO (and CBO) from the natural value. The existence of a clifflike offset is supported by the observation of a similar alignment for Sb_2S_3 and TiO_2 reported elsewhere.[37]

There is a significant difference in how closely matched the natural alignment and Kraut method results are for Sb_2Se_3/CdS and Sb_2Se_3/TiO_2. For the Sb_2Se_3/CdS interface, the difference is minimal. The similitude of sulfur and selenium as anions in terms of both valency and electronegativity could play a part in this. While the electronegativity of all three cations (Ti, Cd, and Sb) are all reasonably similar (1.54, 1.69, and 2.05), the electronegativity of O (3.44) is far greater than those of S and Se (2.58 and 2.55), which are almost equal.[38−40] This means that CdS and Sb_2Se_3 are expected to have a similar overall electronegativity, while the electronegativity of TiO_2 is expected to be significantly greater (there being twice as many O atoms as Ti). A smaller electronegativity difference between the two contacted materials means less charge transfer upon contact and a smaller interface dipole.[38,41]

From a device performance perspective, the results of the band alignment measurements show that the CdS/Sb_2Se_3 interface has a better alignment than TiO_2/Sb_2Se_3—according to the Kraut method, TiO_2 would form a large clifflike barrier at the interface with Sb_2Se_3, leading to a limited available voltage from these kinds of devices. CdS, however, has a conduction band that is perfectly aligned with the conduction band of Sb_2Se_3, showing that this would provide a near-perfect window layer partner, at least in terms of band alignment—a small interfacial spike between 0.3 and 0.4 eV has been shown to be ideal for PV devices with materials such as CZTS and CdTe.[14,35,36] Additionally, the difference between the natural alignment and Kraut method offsets presents some interesting insights into the formation of these interfaces.

Interestingly, however, CdS-based devices do not necessarily perform better than TiO_2-based devices. It has been shown by our group previously that, for Sb_2Se_3 films grown by CSS, the devices utilizing a CdS window layer perform very poorly compared to those using TiO_2.[12] Phillips et al. reported a power conversion efficiency of only 1.44% for a CdS-based device compared to 5.48% for a TiO_2-based device. While the V_{oc} and FF were somewhat lower for CdS (0.42 V and 45.48%) than for TiO_2 (0.45 V and 48.96%), the most significant difference was in the J_{sc}: only 7.57 mA·cm^{-2} for CdS compared to 25.44 mA·cm^{-2} for TiO_2. This is the opposite of what would be expected from the band alignments measured in this study—the clifflike offset of the TiO_2/Sb_2Se_3 interface would be expected to cause a lower V_{oc} than CdS/Sb_2Se_3 and the small CBO of the CdS/Sb_2Se_3 would lead to a very good current. This discrepancy is attributed to interdiffusion of the anions, S and Se, across the interface during the high-temperature growth stage of the Sb_2Se_3 devices, a process which leads to the formation of a CdSe layer between the Sb_2Se_3 and CdS.[12] This is evidenced by time-of-flight secondary ion mass spectrometry and external quantum efficiency measurements by Phillips et al.[12] and significantly reduces the efficiency of the carrier transport from the absorber to the window layer (the intermixing is not present in the samples used for the band alignments measurements as discussed below). This is further illustrated by Williams et al. where the overlapping presence of Cd, S, and Se at the interface as well as the possible presence of metallic Sb is shown with cross-sectional transmission electron microscopy with elemental mapping.[5] The implication of this is that it may be possible to achieve a superior device performance if the interdiffusion can be prevented in such a way that the favorable band alignment between CdS and Sb_2Se_3 can be retained.

While the intermixed region is ever-present in the working devices, it is noted here that intermixing is not expected to occur in the samples presented here. Sb_2Se_3 films deposited by CSS for devices are made via a two-step process, an initial step at lower temperature to lay down a seed layer and then a longer, higher temperature deposition to achieve a good grain size/structure. Given that for the interfacial samples the deposition was only 30 s long and at the lower temperature used to deposit the seed layer, it is assumed that no significant intermixing was able to occur. Additionally, there is no evidence of any additional chemically shifted components in the photoemission spectra that could be attributed to CdSe or Sb_2S_3 in the interface region.

It is noteworthy here that the current record efficiency for any Sb_2Se_3 solar cell is held by Li et al.[8] and that in their study

https://dx.doi.org/10.1021/acsaem.0c01477
ACS Appl. Energy Mater. 2020, 3, 11617−11626

a thin TiO_2 interlayer deposited by atomic layer deposition was used between CdS and Sb_2Se_3 to block a similar interdiffusion process. While it must be acknowledged that the devices made by Li et al. contained a number of differences from the standard Sb_2Se_3 device structure considered in this work (the use of a substrate configuration and a nanorod structure among them), it is promising to the conclusions of this work that to the best of our knowledge the only study in which steps have been taken to prevent the interdiffusion between CdS and Sb_2Se_3 has achieved such outstanding performance. We postulate, therefore, that the band alignments between TiO_2 and Sb_2Se_3 are a limit to the potential efficiency of Sb_2Se_3 devices that use TiO_2 as a window layer. Furthermore, with use of CdS as a window layer (while blocking interdiffusion with an interlayer thin enough not to interfere significantly with the band alignments), the efficiencies of Sb_2Se_3 solar cells could be improved beyond 10%.

CONCLUSION

In this work we have used photoemission techniques to thoroughly study the band alignments between Sb_2Se_3 and two of its most commonly used window layers—CdS and TiO_2. The result of natural alignment measurements showed CdS and Sb_2Se_3 to have a small CBO of 0.36 eV, while the offset between Sb_2Se_3 and TiO_2 CBO was 0.11 eV. Kraut method measurements carried out using HAXPES revealed a similar result for Sb_2Se_3/CdS of −0.01 eV, while the offset for Sb_2Se_3/TiO_2 was significantly different at −0.82 eV. The results suggest that CdS has an optimal band alignment with Sb_2Se_3, while TiO_2-based devices are likely limited by a clifflike offset leading to recombination and a limited built-in voltage. This is especially relevant considering the evidence of detrimental intermixing at CdS/Sb_2Se_3 interfaces. This has led some groups to prefer the use of TiO_2 as a window layer and has also inspired the use of an interdiffusion blocking interlayer in a recent record efficiency publication.[8] The harnessing of advantageous band alignments while preventing interdiffusion could provide a platform for pushing the efficiencies of Sb_2Se_3 to the next level.

ASSOCIATED CONTENT

Supporting Information

The Supporting Information is available free of charge at https://pubs.acs.org/doi/10.1021/acsaem.0c01477.

Tables detailing the binding energies of all fitted core levels and valence bands and the calculated band offsets; graphs showing core level and band edge fits for all photoemission results (PDF)

AUTHOR INFORMATION

Corresponding Author

Tim D. Veal − *Stephenson Institute for Renewable Energy and Department of Physics, University of Liverpool, Liverpool L69 7ZF, United Kingdom;* orcid.org/0000-0002-0610-5626; Email: T.Veal@liverpool.ac.uk

Authors

Huw Shiel − *Stephenson Institute for Renewable Energy and Department of Physics, University of Liverpool, Liverpool L69 7ZF, United Kingdom*

Oliver S. Hutter − *Stephenson Institute for Renewable Energy and Department of Physics, University of Liverpool, Liverpool L69 7ZF, United Kingdom; Department of Mathematics, Physics and Electrical Engineering, Northumbria University, Newcastle upon Tyne NE1 8ST, United Kingdom;* orcid.org/0000-0002-8838-8956

Laurie J. Phillips − *Stephenson Institute for Renewable Energy and Department of Physics, University of Liverpool, Liverpool L69 7ZF, United Kingdom*

Jack E. N. Swallow − *Stephenson Institute for Renewable Energy and Department of Physics, University of Liverpool, Liverpool L69 7ZF, United Kingdom*

Leanne A. H. Jones − *Stephenson Institute for Renewable Energy and Department of Physics, University of Liverpool, Liverpool L69 7ZF, United Kingdom*

Thomas J. Featherstone − *Stephenson Institute for Renewable Energy and Department of Physics, University of Liverpool, Liverpool L69 7ZF, United Kingdom*

Matthew J. Smiles − *Stephenson Institute for Renewable Energy and Department of Physics, University of Liverpool, Liverpool L69 7ZF, United Kingdom;* orcid.org/0000-0003-2530-5647

Pardeep K. Thakur − *Diamond Light Source, Harwell Science & Innovation Campus, Didcot OX11 0DE, United Kingdom;* orcid.org/0000-0002-9599-0531

Tien-Lin Lee − *Diamond Light Source, Harwell Science & Innovation Campus, Didcot OX11 0DE, United Kingdom*

Vinod R. Dhanak − *Stephenson Institute for Renewable Energy and Department of Physics, University of Liverpool, Liverpool L69 7ZF, United Kingdom*

Jonathan D. Major − *Stephenson Institute for Renewable Energy and Department of Physics, University of Liverpool, Liverpool L69 7ZF, United Kingdom*

Complete contact information is available at: https://pubs.acs.org/10.1021/acsaem.0c01477

Notes

The authors declare no competing financial interest.

ACKNOWLEDGMENTS

The Engineering and Physical Sciences Research Council (EPSRC) is acknowledged for funding of H.S. (Grant No. EP/N509693/1), O.S.H. (Grant No. EP/M024768/1), L.A.H.J. (Grant No. EP/R513271/1), J.E.N.S., T.J.F., and M.J.S. (Grant No. EP/L01551X/1), L.J.P. and J.D.M. (Grant No. EP/N014057/1), and V.R.D. and T.D.V. (Grant No. EP/N015800/1). The XRD facility was supported by the EPSRC under Grant No. EP/P001513/1. Paul Warren of the NSG Group is thanked for discussions and funding of H.S. and for supplying coated glass substrates. Diamond Light Source is acknowledged for I09 beam time under proposal SI23160-1.

REFERENCES

(1) Birkett, M.; Linhart, W. M.; Stoner, J.; Phillips, L. J.; Durose, K.; Alaria, J.; Major, J. D.; Kudrawiec, R.; Veal, T. D. Band gap temperature-dependence of close-space sublimation grown Sb_2Se_3 by photo-reflectance. *APL Mater.* **2018**, *6*, 084901.

(2) Chen, C.; Li, W.; Zhou, Y.; Chen, C.; Luo, M.; Liu, X.; Zeng, K.; Yang, B.; Zhang, C.; Han, J.; Tang, J. Optical properties of amorphous and polycrystalline Sb_2Se_3 thin films prepared by thermal evaporation. *Appl. Phys. Lett.* **2015**, *107*, 043905.

(3) Zhou, Y.; Wang, L.; Chen, S.; Qin, S.; Liu, X.; Chen, J.; Xue, D. J.; Luo, M.; Cao, Y.; Cheng, Y.; Sargent, E. H.; Tang, J. Thin-film

Sb_2Se_3 photovoltaics with oriented one-dimensional ribbons and benign grain boundaries. *Nat. Photonics* **2015**, *9*, 409−415.
(4) Hutter, O. S.; Phillips, L. J.; Durose, K.; Major, J. 6.6% efficient antimony selenide solar cells using grain structure control and an organic contact layer. *Sol. Energy Mater. Sol. Cells* **2018**, *188*, 177−181.
(5) Williams, R. E.; Ramasse, Q. M.; McKenna, K. P.; Phillips, L. J.; Yates, P. J.; Hutter, O. S.; Durose, K.; Major, J. D.; Mendis, B. G. Evidence for Self-healing Benign Grain Boundaries and a Highly Defective Sb_2Se_3−CdS Interfacial Layer in Sb_2Se_3 Thin-Film Photovoltaics. *ACS Appl. Mater. Interfaces* **2020**, *12*, 21730−21738.
(6) Luo, M.; Leng, M.; Liu, X.; Chen, J.; Chen, C.; Qin, S.; Tang, J. Thermal evaporation and characterization of superstrate CdS/Sb_2Se_3 solar cells. *Appl. Phys. Lett.* **2014**, *104*, 173904.
(7) Liu, X.; Chen, J.; Luo, M.; Leng, M.; Xia, Z.; Zhou, Y.; Qin, S.; Xue, D.-J.; Lv, L.; Huang, H.; Niu, D.; Tang, J. Thermal evaporation and characterization of Sb_2Se_3 thin film for substrate Sb_2Se_3/CdS solar cells. *ACS Appl. Mater. Interfaces* **2014**, *6*, 10687−10695.
(8) Li, Z.; Liang, X.; Li, G.; Liu, H.; Zhang, H.; Guo, J.; Chen, J.; Shen, K.; San, X.; Yu, W.; Schropp, R. E. I.; Mai, Y. 9.2%-Efficient Core-Shell Structured Antimony Selenide Nanorod Array Solar Cells. *Nat. Commun.* **2019**, *10*, 125.
(9) Wong, L. H.; Zakutayev, A.; Major, J. D.; Hao, X.; Walsh, A.; Todorov, T. K.; Saucedo, E. Emerging inorganic solar cell efficiency tables (Version 1). *J. Physics: Energy* **2019**, *1*, 032001.
(10) Wen, X.; Chen, C.; Lu, S.; Li, K.; Kondrotas, R.; Zhao, Y.; Chen, W.; Gao, L.; Wang, C.; Zhang, J.; Niu, G.; Tang, J. Vapor transport deposition of antimony selenide thin film solar cells with 7.6% efficiency. *Nat. Commun.* **2018**, *9*, 2179.
(11) Wang, L.; Li, D. B.; Li, K.; Chen, C.; Deng, H. X.; Gao, L.; Zhao, Y.; Jiang, F.; Li, L.; Huang, F.; He, Y.; Song, H.; Niu, G.; Tang, J. Stable 6%-efficient Sb_2Se_3 solar cells with a ZnO buffer layer. *Nature Energy* **2017**, *2*, 17046.
(12) Phillips, L. J.; Savory, C. N.; Hutter, O. S.; Yates, P. J.; Shiel, H.; Mariotti, S.; Bowen, L.; Birkett, M.; Durose, K.; Scanlon, D. O.; Major, J. D. Current enhancement via a TiO_2 window layer for CSS Sb_2Se_3 solar cells: performance limits and high V_{oc}. *IEEE J. Photovoltaics* **2019**, *9*, 544−551.
(13) Ding, C.; Zhang, Y.; Liu, F.; Kitabatake, Y.; Hayase, S.; Toyoda, T.; Yoshino, K.; Minemoto, T.; Katayama, K.; Shen, Q. Effect of the conduction band offset on interfacial recombination behavior of the planar perovskite solar cells. *Nano Energy* **2018**, *53*, 17−26.
(14) Kephart, J.; McCamy, J.; Ma, Z.; Ganjoo, A.; Alamgir, F.; Sampath, W. Band alignment of front contact layers for high-efficiency CdTe solar cells. *Sol. Energy Mater. Sol. Cells* **2016**, *157*, 266−275.
(15) Wallace, S. K.; Butler, K. T.; Hinuma, Y.; Walsh, A. Finding a junction partner for candidate solar cell absorbers enargite and bournonite from electronic band and lattice matching. *J. Appl. Phys.* **2019**, *125*, 055703.
(16) Helander, M.; Greiner, M.; Wang, Z.; Lu, Z. Pitfalls in measuring work function using photoelectron spectroscopy. *Appl. Surf. Sci.* **2010**, *256*, 2602−2605.
(17) Schlaf, R.; Murata, H.; Kafafi, Z. Work function measurements on indium tin oxide films. *J. Electron Spectrosc. Relat. Phenom.* **2001**, *120*, 149−154.
(18) Kraut, S.; Grant, E. A.; Waldrop, J. R.; Kowalczyk, S. P. Precise determination of the valence band edge in x-ray photoemission spectra: application to measurement of semiconductor interface potentials. *Phys. Rev. Lett.* **1980**, *44*, 1620−1623.
(19) King, P. D. C.; Veal, T. D.; Kendrick, C. E.; Bailey, L. R.; Durbin, S. M.; McConville, C. F. InN/GaN valence band offset: High-resolution x-ray photoemission spectroscopy measurements. *Phys. Rev. B: Condens. Matter Mater. Phys.* **2008**, *78*, 033308.
(20) Anderson, R. L. Germanium-Gallium Arsenide Heterojunctions [Letter to the Editor]. *IBM J. Res. Dev.* **1960**, *4*, 283−287.
(21) Mariotti, S.; Hutter, O. S.; Phillips, L. J.; Yates, P. J.; Kundu, B.; Durose, K. Stability and performance of $CsPbI_2Br$ thin films and solar cell devices. *ACS Appl. Mater. Interfaces* **2018**, *10*, 3750−3760.
(22) Burton, L. A.; Whittles, T. J.; Hesp, D.; Linhart, W. M.; Skelton, J. M.; Hou, B.; Webster, R. F.; O'Dowd, G.; Reece, C.; Cherns, D.; Fermin, D. J.; Veal, T. D.; Dhanak, V. R.; Walsh, A. Electronic and optical properties of single crystal SnS_2: an earth-abundant disulfide photocatalyst. *J. Mater. Chem. A* **2016**, *4*, 1312−1318.
(23) Klein, A. Energy band alignment at interfaces of semiconducting oxides: A review of experimental determination using photoelectron spectroscopy and comparison with theoretical predictions by the electron affinity rule, charge neutrality levels, and the common anion rule. *Thin Solid Films* **2012**, *520*, 3721−3728. Seventh International Symposium on Transparent Oxide Thin Films for Electronics and Optics (TOEO-7).
(24) Klein, A. Energy band alignment in chalcogenide thin film solar cells from photoelectron spectroscopy. *J. Phys.: Condens. Matter* **2015**, *27*, 134201.
(25) Niles, D. W.; Margaritondo, G. Heterojunctions: Definite breakdown of the electron affinity rule. *Phys. Rev. B: Condens. Matter Mater. Phys.* **1986**, *34*, 2923−2925.
(26) Schlaf, R.; Lang, O.; Pettenkofer, C.; Jaegermann, W. Band lineup of layered semiconductor heterointerfaces prepared by van der Waals epitaxy: Charge transfer correction term for the electron affinity rule. *J. Appl. Phys.* **1999**, *85*, 2732−2753.
(27) Li, D.-B.; Yin, X.; Grice, C. R.; Guan, L.; Song, Z.; Wang, C.; Chen, C.; Li, K.; Cimaroli, A. J.; Awni, R. A.; Zhao, D.; Song, H.; Tang, W.; Yan, Y.; Tang, J. Stable and efficient CdS/Sb_2Se_3 solar cells prepared by scalable close space sublimation. *Nano Energy* **2018**, *49*, 346−353.
(28) Shiel, H.; Hutter, O. S.; Phillips, L. J.; Turkestani, M. A.; Dhanak, V. R.; Veal, T. D.; Durose, K.; Major, J. D. Chemical etching of Sb_2Se_3 solar cells: surface chemistry and back contact behaviour. *J. Physics: Energy* **2019**, *1*, 045001.
(29) Tanuma, S.; Powell, C. J.; Penn, D. R. Calculation of electron inelastic mean free paths (IMFPs) VII. Reliability of the TPP-2M IMFP predictive equation. *Surf. Interface Anal.* **2003**, *35*, 268−275.
(30) Hutter, O. S.; Phillips, L. J.; Yates, P. J.; Major, J. D.; Durose, K. CSS antimony selenide film morphology and high efficiency PV devices. *WCPEC-7 Conference Paper* **2018**, 0027−0031.
(31) Dette, C.; Pérez-Osorio, M. A.; Kley, C. S.; Punke, P.; Patrick, C. E.; Jacobson, P.; Giustino, F.; Jung, S. J.; Kern, K. TiO_2 Anatase with a Bandgap in the Visible Region. *Nano Lett.* **2014**, *14*, 6533−6538.
(32) Whittles, T. J.; Veal, T. D.; Savory, C. N.; Welch, A. W.; de Souza Lucas, F. W.; Gibbon, J. T.; Birkett, M.; Potter, R. J.; Scanlon, D. O.; Zakutayev, A.; Dhanak, V. R. Core Levels, Band Alignments, and Valence-Band States in $CuSbS_2$ for Solar Cell Applications. *ACS Appl. Mater. Interfaces* **2017**, *9*, 41916−41926.
(33) Oliva, A.; Solís-Canto, O.; Castro-Rodríguez, R.; Quintana, P. Formation of the band gap energy on CdS thin films growth by two different techniques. *Thin Solid Films* **2001**, *391*, 28−35.
(34) Hobson, T. D. C.; Phillips, L. J.; Hutter, O. S.; Shiel, H.; Swallow, J. E. N.; Savory, C. N.; Nayak, P. K.; Mariotti, S.; Das, B.; Bowen, L.; Jones, L. A. H.; Featherstone, T. J.; Smiles, M. J.; Farnworth, M. A.; Zoppi, G.; Thakur, P. K.; Lee, T.-L.; Snaith, H. J.; Leighton, C.; Scanlon, D. O.; Dhanak, V. R.; Durose, K.; Veal, T. D.; Major, J. D. Isotype Heterojunction Solar Cells Using n-Type Sb_2Se_3 Thin Films. *Chem. Mater.* **2020**, *32*, 2621−2630.
(35) Bechlaghem, S.; Zebentout, B.; Benamara, Z. The major influence of the conduction-band-offset on Zn(O,S)/$CuIn_{0.7}Ga_{0.3}Se_2$ solar cells. *Results Phys.* **2018**, *10*, 650−654.
(36) Pudov, A. O.; Kanevce, A.; Al-Thani, H. A.; Sites, J. R.; Hasoon, F. S. Secondary barriers in CdS-$CuIn_{1-x}Ga_xSe_2$ solar cells. *J. Appl. Phys.* **2005**, *97*, 064901.
(37) Prabhakar, R. R.; Moehl, T.; Siol, S.; Suh, J.; Tilley, S. D. Sb_2S_3/TiO_2 Heterojunction Photocathodes: Band Alignment and Water Splitting Properties. *Chem. Mater.* **2020**, *32*, 7247.
(38) Mönch, W. *Semiconductor Surfaces and Interfaces*; Springer: 1993; p 548.

https://dx.doi.org/10.1021/acsaem.0c01477
ACS Appl. Energy Mater. 2020, 3, 11617−11626

(39) Miedema, A. R.; de Boer, F. R.; de Chatel, P. F. Empirical description of the role of electronegativity in alloy formation. *J. Phys. F: Met. Phys.* **1973**, *3*, 1558−1576.
(40) Miedema, A.; de Châtel, P.; de Boer, F. Cohesion in alloys - fundamentals of a semi-empirical model. *Physica B+C* **1980**, *100*, 1−28.
(41) Mönch, W. *Electronic Properties of Semiconductor Interfaces*; Springer: 1986; p 263.

https://dx.doi.org/10.1021/acsaem.0c01477
ACS Appl. Energy Mater. 2020, 3, 11617−11626